Strontium isotope fractionation during strontianite ($SrCO_3$) dissolution, precipitation and at equilibrium

Vasileios Mavromatis[1,2,*], Anna L. Harrison[2], Anton Eisenhauer[3], Martin Dietzel[1]

[1]Institute of Applied Geosciences, Graz University of Technology, Rechbauerstr. 12, A-8010 Graz, Austria

[2]Géosciences Environnement Toulouse (GET), CNRS, UMR5563, 14 Avenue Edouard Belin, 31400, Toulouse, France

[3] GEOMAR Helmholtz Centre for Ocean Research Kiel, Wischhofstr. 1-3, D-24148 Kiel, Germany

*Corresponding author Email: mavromatis@tugraz.at

Abstract

In this study we examine the behavior of stable Sr isotopes between strontianite [$SrCO_3$] and reactive fluid during mineral dissolution, precipitation, and at chemical equilibrium. Experiments were performed in batch reactors at 25°C in 0.01 M NaCl solutions wherein the pH was adjusted by bubbling of a water saturated gas phase of pure CO_2 or atmospheric air. The equilibrium Sr isotope fractionation between strontianite and fluid after dissolution of the solid under 1 atm CO_2 atmosphere was estimated as $\Delta^{88/86}Sr_{SrCO3\text{-}fluid} = \delta^{88/86}Sr_{SrCO3} - \delta^{88/86}Sr_{fluid} = -0.05\pm0.01$‰. On the other hand, during strontianite precipitation, an enrichment of the fluid phase in ^{88}Sr, the heavy isotopomer, was observed. The evolution of the $\delta^{88/86}Sr_{fluid}$ during strontianite precipitation can be modeled using a Rayleigh distillation approach and the estimated, kinetically driven, fractionation factor $\alpha_{SrCO3\text{-}fluid}$ between solid and fluid is calculated to be 0.99985 ± 0.00003 corresponding to $\Delta^{88/86}Sr_{SrCO3\text{-}fluid} = -0.15$‰. The obtained results further support that under chemical equilibrium conditions between solid and fluid a continuous exchange of isotopes occurs until the system approaches isotopic equilibrium. This isotopic exchange is not limited to the outer surface layer of the strontianite crystal, but extends to ~7-8 unit cells below the crystal surface. The behavior of Sr isotopes in this study is in excellent agreement with the concept of dynamic equilibrium and it suggests that the time needed for achievement of chemical equilibrium is generally shorter compared to that for isotopic equilibrium. Thus it is suggested that in natural Sr-bearing carbonates an isotopic change may still occur close to thermodynamic equilibrium, despite no observable change in aqueous elemental concentrations. As such, a secondary and ongoing change of Sr isotope signals in carbonate minerals caused by isotopic re-equilibration with fluids has to be considered in order to use Sr isotopes as environmental proxies in aquatic environments.

1. Introduction

The ability to routinely measure the isotopic composition of a plethora of elements in geological material with very high precision marked a new era for geochemistry. Today, stable isotopes of major and trace elements are used to reconstruct paleo-environmental conditions (*e.g.*, Rollion-Bard et al., 2011; Böhm et al., 2012; Shirokova et al., 2013; Geske et al., 2015; Vigier et al., 2015; Noireaux et al., 2015), to understand weathering processes (*e.g.*, Mavromatis et al., 2014; 2016a; Pokrovsky et al., 2011; Beinlich et al., 2014), to study diagenetic alteration (*e.g.*, Riechelmann et al., 2016; Rollion-Bard et al., 2016), and to trace anthropogenic activity (*e.g.*, Dietzel et al., 2016; Heuser and Eisenhauer, 2010). The use of stable isotope compositions of secondary minerals, however, demands knowledge of whether mineral formation occurred close to or far from chemical equilibrium. This is because at low temperatures kinetic isotope fractionation effects that usually occur during precipitation at far from equilibrium conditions, can generate isotopic compositions of carbonate minerals that differ significantly from isotope equilibrium compositions (Tang et al., 2008a; Mavromatis et al., 2017a). In contrast at higher temperatures kinetic isotope effects occurring during mineral growth would be erased as chemical and isotopic equilibrium between solid and fluid is achieved rather fast (Pearce et al., 2012; Beinlich et al., 2014).

To date it has been well established in a large number of experimental studies that mineral growth rate is one of the parameters that strongly affects isotopic fractionation (*e.g.*, Skulan et al., 2002; Tang et al., 2008a; Eisenhauer et al., 2009, Immenhauser et al., 2010). When it comes to carbonate minerals, that are regularly used by the scientific community to track environmental conditions in the geological past, the number of experimental studies mapping kinetic isotope effects are a minority in the isotope literature (Li et al., 2012; Tang et al., 2008a, 2012; Böhm et al., 2012; Immenhauser et al., 2010; Fruchter et al., 2016). Even smaller is the number of experimental works studying isotope fractionation under near to thermodynamic equilibrium conditions in carbonates at low temperature (Mavromatis et al.,

2013; 2017a; 2017b; Li et al., 2011; 2014; 2015). On the other hand, the improved capability of computational calculations in recent years, has allowed for an increase in the number of studies that estimate isotopic fractionation at equilibrium based on theoretical calculations (Schauble, 2011; Rustad et al., 2010; Meheut et al., 2007; Pinilla et al., 2015; Schott et al., 2016). Comparison of these modelling results with the outcome of experimental studies, however, suggests that a significant discrepancy between measurements and theoretical calculations persists. A good example is the Mg isotopic fractionation between magnesite and fluid (Pearce et al., 2012; Schauble, 2011; Rustad et al., 2010), Mg-calcite and fluid (Mavromatis et al., 2013; Pinilla et al., 2015), and brucite and fluid (Li et al., 2014; Schott et al., 2016). For example the measured Mg isotope fractionation between magnesite and reactive fluid at 200^{o}C reported by Pearce et al. (2012) to be -0.88‰, whereas that predicted by ab-initio calculations varies between -0.50‰ (Rustad et al., 2010) and -1.75‰ (Schauble, 2011).

Knowledge of both the isotopic equilibrium and the effect of mineral growth kinetics on isotope fractionation factors is essential in order to use the stable isotope composition of secondary minerals for (paleo)environmental or forensic tasks. This holds true not only for the stable isotopes of the constituting elements of readily forming Ca- and Mg-bearing carbonate minerals in Earth's surface environments, but also for the stable isotopes of divalent metal cations (Me^{2+}) that are commonly incorporated into the Ca-bearing carbonates. Such elements form individual carbonate minerals (e.g., $BaCO_3$, $SrCO_3$, $ZnCO_3$) under specific ambient environmental conditions but are also common constituents of solid-solutions with $CaCO_3$ minerals. The experimental investigation of the isotopic fractionation behavior between these minerals and an aqueous fluid (i) provides the basis for further development and/or validation of theoretical calculations, (ii) gives insights into the isotope behavior during the formation of solid-solutions, and (iii) sheds light on the mechanisms controlling isotopic fractionation during both formation of endmember Me^{2+} carbonate minerals and incorporation of the Me^{2+}

in carbonate mineral solid-solutions (e.g. the strontianite-aragonite solid-solution series; Plummer and Busenberg, 1987; Plummer et al., 1992).

In the present study we examine the fractionation of stable Sr isotopes between strontianite [$SrCO_3$] and reactive fluid. Strontium is an impurity in calcite and usually present in natural aragonites at high concentrations, owing to the isostructural crystallization of aragonite and strontianite and the formation of an ideal solid-solution at the aragonite endpoint (Speer, 1983). Stable strontium isotope fractionation has been investigated during calcite (Böhm et al., 2012; AlKhatib and Eisenhauer, 2017a) and aragonite growth (Fruchter et al., 2016; AlKhatib and Eisenhauer, 2017b) in laboratory studies. Herein we focus on the formation of pure $SrCO_3$ following the previous works on $MgCO_3$ (Pearce et al., 2012) and $BaCO_3$ (Mavromatis et al., 2016b) in an effort to expand the existing knowledge on the behavior of stable isotope fractionation of divalent cations of their pure Me-carbonate mineral phase during dissolution, precipitation, and at equilibrium. In this study, the Sr isotopic evolution of the reactive solution during strontianite dissolution and precipitation was measured, with particular attention paid to the isotopic evolution following attainment of chemical equilibrium of the reactive fluid with respect to strontianite. The experimental results are discussed in the context of isotope (dis-) equilibrium phenomena, the potential secondary resetting of the Sr isotope signal in the Sr-endmember carbonate mineral strontianite, and the utility of Sr isotopes as an environmental proxy.

2. Materials and Methods

2.1 Experimental materials

The methodology followed for strontianite synthesis is similar to that reported previously by Mavromatis et al. (2016b) for synthesis of witherite ($BaCO_3$). Briefly, pure strontianite seeds were produced by mixing equimolar $SrCl_2$ and Na_2CO_3 solutions prepared from analytical grade chemicals (Sigma-Aldrich) in deionized water, and placing the slurry

into a stirred titanium Parr reactor (series 4560). The reactor was sealed and the temperature and pCO_2 adjusted to 200°C and 15 bars, respectively. The solids were recovered after 30 days of reaction time, rinsed in deionized water, and dried at room temperature. The synthesis of seed crystals with this technique provides chemical and isotopic homogeneity in the precipitated carbonate, as is evident from the amount of Sr remaining in the aqueous phase, at < 0.1 % of the total mass of Sr introduced initially. This is further supported by the $\delta^{88/86}Sr$ isotopic composition of the bulk strontianite (*i.e.*, $\delta^{88/86}Sr = 0.145 \pm 0.003$), which is identical to that of the initial $SrCl_2$ solution (i.e., $\delta^{88/86}Sr = 0.154 \pm 0.013$) within analytical error (Table 1). Note here that Skulan et al. (2002) postulated achievement of equilibrium in Fe isotopes between hematite and fluid at 98°C after ~40 days of incubation time, suggesting that the method followed for the formation of strontianite likely results to an isotopic homogeneous solid.

The synthesized strontianite consisted of 0.1-2.0 μm euhedral crystals (Fig. 1). The mineralogy of these crystals was confirmed by X-ray diffraction (XRD) analysis. The specific surface area of the synthetic strontianite powder determined by multi-point krypton adsorption BET method (Brunauer et al., 1938) using a Quantachrome Autosorb-1MP, was 1.1 ± 0.1 m^2/g.

2.2 Dissolution/Precipitation experiments

The experimental set up for strontianite dissolution and precipitation makes use of the pH dependent solubility of carbonate minerals to induce dissolution and precipitation in separate steps within the same reactor, and is described in detail by Mavromatis et al. (2016b). The pH of the aqueous fluid was controlled by continuous bubbling of a water-saturated gas phase through the reactors throughout the experimental runs. The experimental set up can be seen in Fig. 2. At the onset of the experimental run, approximately 5 g of synthetic strontianite were placed in a 1.2 L Nalgene batch reactor containing ~1.1 L of a 10^{-2} M NaCl

143 aqueous solution (refer to Electronic Supplementary Material-ESM Table 1). Within this
144 study, two identical experiments were performed in order to control the reproducibility of the
145 reaction mechanisms and kinetics of the experimental runs. Reactors were equipped with a
146 floating stir bar rotating at 300 rpm (Fig. 2). The experimental setup was placed in a room
147 with a constant temperature of 25±1 ^{o}C. Strontianite dissolution during phase I of the
148 experimental runs was initiated by bubbling pure CO_2 (1 atm) through the reactor. This kept
149 the pH of the fluid at a quasi-constant value of about six. A subsequent change of the
150 bubbling gas phase from pure CO_2 to atmospheric air marked the onset of phase II and
151 resulted in the fluid becoming oversaturated with respect to strontianite due to CO_2 degassing
152 and an increase in pH. This initiated strontianite precipitation until a second chemical
153 equilibrium was attained according to the reaction:
154 $Sr^{2+} + CO_3^{2-} \leftrightharpoons SrCO_3$ ($K_{strontianite}$: $10^{-9.27}$; Busenberg et al., 1984) (1)
155 This new chemical equilibrium was achieved at a pH value of approximately 8 (Fig. 2). In
156 order to minimize evaporation, gases were bubbled through a 10^{-2} M NaCl solution prior to
157 their introduction in the reaction vessel (Fig. 2). Fluid samples of known quantity were taken
158 at regular time intervals throughout the experiment using a syringe. Stirring of the fluid was
159 stopped shortly prior to sampling to allow the strontianite to settle. In this way solid removal
160 was minimized and the solid-to-solution ratio was precisely monitored during the course of
161 each experiment. This protocol provided precise knowledge of Sr mass distribution (*i.e.*,
162 between fluid phase, solid phase and retrieved sample). At the end of phase I and prior to
163 change of the gas phase, a few grains of the strontianite present in the reactors were removed
164 for isotopic analysis. The removal of this material did not significantly alter the mass of solid
165 present in the reactor and is not considered in the calculations presented hereafter.
166 Immediately after sampling, the fluid was filtered through a 0.2 μm cellulose acetate
167 membrane syringe filter and a sub-sample was acidified for Sr concentration and isotopic
168 measurements. Reactive fluid carbonate alkalinity was determined in a second sub-sample,

and fluid pH was measured *in situ* in the reactors. At the end of the experimental run, the entire reactive fluid was vacuum filtered through a 0.2 μm membrane (Sartorius, cellulose acetate). The solids were rinsed with MilliQ water and dried at room temperature.

2.3 Solid and fluid phase characterization

Strontium concentrations were measured by inductively-coupled plasma optical emission spectrometry (ICP-OES) using a Perkin Elmer Optima ICP-OES 4300. The statistical uncertainty is reported as two standard deviations (2σ) in the concentration range of 0.01 – 0.17 $x10^{-3}$ M corresponding to ±3%. The total alkalinity of the reactive fluids was determined by a Schott TitroLine alpha plus titrator with an uncertainty of ±2% and a detection limit of 5 $x10^{-6}$ M. Fluid pH was measured with a Schott Blueline 28 combined electrode, calibrated with NIST standard buffers at pH of 4.01, 7.00 and 10.00, and with an uncertainty of ± 0.03 pH units. The calibration of the pH-meter took place shortly prior to each sample collection and pH measurements performed in-situ.

X-ray diffraction analyses of synthetic strontianite was performed using a PANalytical X`Pert PRO diffractometer equipped with a Scientific X'Celerator detector and a Co-target tube operated at 40 kV and 40 mA. The 2θ angle range was set to 4 to 85° using a step size of 0.008° 2θ and a count time of 40 s/step. Scanning Electron Microscopy (SEM) observations of solids were performed after gold-coating using a ZEISS DSM 982 Gemini microscope operating at 5 kV accelerating voltage.

Aqueous speciation and the saturation state ($\Omega_{strontianite} = IAP/K_{sp,strontianite}$) of the reacting fluids with respect to strontianite were calculated using the PHREEQC software together with its MINTEQ V4 database (Parkhurst and Appelo, 1999).

2.4 Strontium isotope analyses

Stable strontium isotope ($\delta^{88/86}Sr$) measurements of liquid and selected solid samples were measured on a Finnigan Triton Thermal Ionization Mass Spectrometer (TIMS) at GEOMAR mass-spectrometer facilities in Kiel using the $^{87}Sr/^{84}Sr$ double spike method (Krabbenhöft et al., 2009). Each sample was separated into two aliquots. The double spike was added to one aliquot (spiked) and the other aliquot was left unspiked. Sr was separated from the matrix solution of each aliquot using the strontium-selective chromatographic resin Eichrom Sr-spec (50–100 mesh) that is loaded in a 650 ll BIO-RAD column tube. The recovery for Sr separation was better than 90%. In each batch of carbonate sample measurements, the JCp-1 standard was also prepared and analyzed repeatedly ($\delta^{88/86}Sr$ = 0.20 ± 0.02‰, 2SD, n = 10) using the same protocol as used for the unknown samples. The IAPSO Seawater Standard (batch ID. P152) was measured in batches of seawater sample measurements ($\delta^{88/86}Sr$ = 0.39 ± 0.02‰, 2SD, n = 4). No blank correction was needed since the total procedural Sr blanks were about 0.04 ng, which is insignificant compared to the amount of Sr in the measured samples (300–700 ng). Sr isotopic values are presented in the standard δ-notation relative to SRM987 as the standard (at value of $^{88}Sr/^{86}Sr$ = 8.375209).

$$\delta^{88/86}Sr = \left(\frac{{}^{88}Sr/{}^{86}Sr_{sample}}{{}^{88}Sr/{}^{86}Sr_{SRM987}} - 1\right) \times 1000 \quad (2)$$

The $\delta^{88/86}Sr$ is presented with an uncertainty of two standard deviations (2σ), as obtained from the external long-term reproducibility of measurements of the JCp-1 coral standard, all seawater samples (of approximately constant $^{88}Sr/^{86}Sr$ composition), and the IAPSO standard. The measurements of both JCp-1and seawater (including the IAPSO seawater standard), yielded an identical external reproducibility of 0.02‰ (2SD).

3. Results

3.1 Strontianite dissolution and precipitation

The measured concentrations of Sr and alkalinity in the reactive fluid during the experimental runs are reported in Table 1 and ESM Table 2 for both replicate experiments. In Fig. 3 the temporal evolution of Sr concentration is plotted together with the evolution of aqueous pH. The observed behavior during phase I of the experimental runs is consistent with the initial dissolution of strontianite and the achievement of chemical equilibrium between strontianite and fluid. The achievement of chemical equilibrium at the onset of phase I, when pure CO_2 was bubbled through the reactors, occurred before the first sample was removed at 1500 min. During these first 1500 min ~16% of the strontianite initially introduced in the reactor was dissolved. The achievement of equilibrium was confirmed by the quasi-constant aqueous Sr and alkalinity concentrations in duplicate experiments during phase I (Table 1). Conversely, at the beginning of phase II, precipitation was induced via bubbling of atmospheric air, which drove an increase in fluid pH and thus the saturation state with respect to strontianite (Table 1). Strontianite precipitation rapidly removed Sr from solution and reduced alkalinity (Fig. 3). A second chemical equilibrium between strontianite and fluid was then achieved within ~420 min (Table 1), as evidenced by near constant pH and Sr concentrations (Fig. 3).

The temporal evolution of strontianite growth rate, r_p, during its precipitation can be assessed by aqueous Sr mass balance in the system and is described by:

$$r_p = \frac{n_{Sr,t_i} - n_{Sr,t_{i-1}}}{t_i - t_{i-1}} / S \qquad (3)$$

where n_{Sr,t_i} are the moles of Sr in the fluid at time t_i, and S refers to the total surface area of strontianite in m^2, which was calculated based on the mass of strontianite present in the reactor and the BET surface area of the strontianite. Thus, r_p is expressed in $mol/m^2/s$. Rates were calculated between sampling points. The total surface area, S, was corrected for the amount of strontianite dissolved or precipitated during the experimental runs and assuming surface area increased proportionally to the mass change and BET measured surface area.

Details on Sr mass balance in the reactor and evolution of the reactive surface can be found in Table ESM 1. The strontianite growth rate during its precipitation exhibits an initial increase of ~3 orders of magnitude in the range of $10^{-11} < r_p < 10^{-8}$ mol/m^2/s (Table 1) which is followed by a decrease after 13020 min elapsed time as chemical equilibrium is approached.

3.2 Sr isotopic composition of fluids and solids

The measured $\delta^{88/86}Sr_{fluid}$ values are given in Table 1 and illustrated in Fig. 4. The strontianite seed crystals ($\delta^{88/86}Sr_{seed}$ = 0.145±0.003 ‰), the $SrCl_2$ solution from which the seed crystals were synthesized ($\delta^{88/86}Sr_{SrCl2}$ = 0.154 ± 0.013 ‰) and the strontianite collected at the end of the experimental run ($\delta^{88/86}Sr_{SrCO3\text{-}end}$ = 0.154 ± 0.002 ‰) have the same isotopic composition within analytical error. The radiogenic ($^{87}Sr/^{86}Sr$) isotope composition of all material used in this study exhibit the same composition as shown in Table 1. The stable isotope composition of strontianite that remained in the reactor during phase I and collected at 12540 min of reaction time exhibits an enrichment in ^{88}Sr ($\delta^{88/86}Sr_{strontianite\text{-}phI}$ = 0.167 ± 0.004 ‰). The isotopic composition of the reactive fluid during phase I of the experiment was constant within analytical uncertainty, and exhibited a value of $\delta^{88/86}Sr_{fluid}$=0.194 ± 0.006 ‰ (n=5), indicative of isotopic steady state in the strontianite-fluid system. After the end of phase I, strontianite precipitation occurred between 12660 and 13400 min, causing a significant increase in $\delta^{88/86}Sr_{fluid}$ from 0.194 ‰ to 0.622 ‰ (Fig. 4). This is attributed to the preferential incorporation of ^{86}Sr in the precipitating strontianite, which effectively enriches the fluid in ^{88}Sr. After the pH-jump, both the pH of the reactive fluid and the aqueous Sr concentration are quasi-constant at ~8.0 and 0.18 mM, respectively within ~420 min (see Fig. 3). Yet, the $\delta^{88/86}Sr_{fluid}$ value is progressively evolving towards lower values up to ~22500 min of reaction time (Fig. 4). This continuing $\delta^{88/86}Sr_{fluid}$ change in the fluid phase indicates that there is ongoing isotopic exchange between the solid and the aqueous phase, despite the achievement of chemical equilibrium.

4. Discussion

4.1 Sr isotope fractionation during strontianite dissolution and precipitation

4.1.1 Strontianite dissolution

The $\delta^{88/86}Sr_{fluid}$ values during the chemical equilibrium achieved in phase I are ~0.05 ‰ higher compared to that of the strontianite seed material (Fig. 4). The observed difference between $\delta^{88/86}Sr_{fluid}$ and $\delta^{88/86}Sr_{strontianite}$ can be attributed to achievement of isotopic equilibrium in the strontianite-fluid system during phase I of the experimental run. The first measurement of the fluid occurred after chemical equilibrium was already achieved; therefore detailed information regarding Sr fractionation during strontianite dissolution cannot be extracted from this dataset. The rather fast achievement of isotopic equilibrium following dissolution, however, is consistent with the behaviour of Ba isotopes in the witherite-fluid system at 25^{o}C (Mavromatis et al., 2016b). This is also expected due to the fast exchange of water molecules between the Sr hydration sphere and the bulk fluid (*i.e.*, 10^{9} s^{-1}; Lincoln and Merbach, 1995), a parameter that is suggested to control isotopic fractionation between mineral and fluid (Gussone et al. 2003, Pearce et al., 2012; Mavromatis et al., 2013). The preferential enrichment of the fluid phase in ^{88}Sr versus the solid that was observed during phase I of the experimental run is consistent with the shorter Sr-O bond length observed in strontianite (2.61 Å; O'Day et al., 2000) compared to that in the aqueous phase (i.e. 2.60 Å; D'Angelo et al., 2016). The small but measureable stable Sr isotope fractionation observed between strontianite and reactive fluid that averages at -0.05 ‰ is comparable to that observed for Mg isotopes during magnesite dissolution and subsequent chemical equilibrium demonstrated by Pearce et al. (2012) in experiments performed at 120 and 150^{o}C. In contrast, in the witherite-fluid system, investigated by Mavromatis et al. (2016b), no significant stable Ba isotope fractionation was observed during the achievement of chemical and isotopic equilibrium. In this latter case it was argued that the absence of measureable fractionation of

295 stable Ba isotopes between witherite and fluid at chemical equilibrium might stem from the
296 small difference in the Ba-O bond length between witherite (i.e. 2.80 Å; Holl et al., 2000) and
297 the aqueous Ba octahedron (i.e 2.79 Å; Persson et al., 1995). Indeed the Me-O bond lengths in
298 strontianite and magnesite are longer compared to the respective aqueous Me^{2+} species, which
299 may lead to observed greater degree of fractionation.
300
301 *4.1.2 Strontianite precipitation*
302 Strontianite precipitation occurred between 12500 and 13000 min of elapsed time
303 when aqueous pH increased from ~6 to ~8 as seen in Fig. 3. This pH increase was driven by
304 changing the supplied gas from pure CO_2 to laboratory atmosphere (~0.05%), and resulted in
305 an increase of the supersaturation of the reactive fluid with respect to strontianite ($\Omega \approx 2.7$;
306 Table 1), and significant removal of Sr from the fluid phase to the solid. The invoked pH-
307 jump forced the system to attain a second chemical equilibrium (phase II). Unlike phase I,
308 however, measurable changes in the $\delta^{88/86}Sr_{fluid}$ were observed throughout phase II (Fig. 4).
309 The fluid became significantly enriched in ^{88}Sr (Fig. 4), indicating a preferential uptake of the
310 lighter ^{86}Sr into the precipitating strontianite. Owing to the closed system behavior of Sr in
311 this experimental setup, the extent of stable Sr isotope fractionation during strontianite
312 precipitation can be estimated using a Rayleigh-type equation (Criss, 1999) where the
313 fractionation factor α between strontianite and reactive fluid is defined as:

314 $$\alpha_{strontianite-fluid} = \frac{\log\left(\frac{1000+\delta^{88/86}Sr_{inst}}{1000+\delta^{88/86}Sr_{init}}\right)}{\log F} + 1 \qquad (4)$$

315 where $\delta^{88/86}Sr_{init}$ and $\delta^{88/86}Sr_{inst}$ are the Sr isotope composition of the reactive fluid during
316 phase I (average $\delta^{88/86}Sr_{fluid}$ = 0.194±0.006‰; n=5) and throughout the precipitation period
317 (i.e. ~12500 – 13000 min, 0.2 > $\delta^{88/86}Sr_{fluid}$ > 0.62; Fig. 4), respectively. *F* is the molar
318 fraction of Sr remaining in the reactive fluid. At *F* = 0.052 (see ESM Table 1) $\delta^{88/86}Sr_{inst}$ is

0.62 ‰, representing the $\delta^{88/86}Sr_{fluid}$ at the beginning of phase II and at the end of the pH-jump. A fractionation factor $\alpha_{strontianite\text{-}fluid}$ at this point in the experiment is estimated to be 0.99987, which corresponds to $\Delta^{88/86}Sr_{strontianite\text{-}fluid} \approx -0.13$ ‰. The mass of Sr removed via sampling compared to that in the reactive fluid is ~3 orders of magnitude lower (ESM Table 1), and thus does not affect the results of Eq. 4. Note here that the estimated α value using Eq. (4) refers to strontianite precipitation between 12540 and 13380 min elapsed time. The $\Delta^{88/86}Sr_{strontianite\text{-}fluid}$ value, however, can also be estimated by fitting all the measured data for the aqueous fluid in phase I and during strontianite precipitation, as is illustrated in Fig. 5. Indeed the Rayleigh curve fitted in Fig. 5 provides an $\alpha_{strontianite\text{-}fluid}$ value of 0.99985 (or $\Delta^{88/86}Sr_{strontianite\text{-}fluid} \approx -0.15$‰). Likely this slight difference in calculated α values occurs due to statistical treatment of the data, as in the case of Eq. (4), only two measured values at 12540 min and 13380 min were taken into account during the calculation, whereas for the Rayleigh-type fractionation fit all data points during phase I and during strontianite precipitation (t = 1500–13380 min; n = 10) were considered. The observed enrichment of strontianite in the lighter ^{86}Sr isotopomer is overall in good agreement with the behavior of alkali earth metals during the precipitation of pure metal-carbonate phases (*e.g.,* Böttcher et al., 2012; Pearce et al., 2012; Tang et al., 2008b; Eisenhauer et al., 2009, Mavromatis et al., 2012a; 2016b; Shirokova et al., 2013; Li et al., 2015). Similar is the case for the incorporation of alkaline earths in $CaCO_3$ minerals as traces or impurities (*e.g.*, Li et al., 2012; Mavromatis et al., 2013; 2017a; 2017b; Böhm et al., 2012; Immenhauser et al., 2010; Fruchter et al., 2016)

In contrast to divalent cation isotope fractionation at equilibrium that can be estimated by thermodynamic considerations of the solid structure and the aqueous species in the fluid phase (Schauble 2011; Rustad et al., 2010; Schott et al., 2016; Pinilla et al., 2015), isotopic fractionation during mineral growth at far from equilibrium conditions is neither well understood nor adequately modeled. There are two models designed to simulate isotopic fractionation during calcite growth; 1) the growth entrapment model (GEM), and 2) the

surface reaction kinetic model (SRKM). The growth entrapment model, developed by Watson and coworkers (Watson and Liang, 1995; Watson, 1996; 2004), suggests the presence of a chemically and isotopically distinct surface layer that is in contact with the reactive fluid and can be either enriched or depleted in an isotopomer or a trace element. The GEM assumes that this reactive layer at the calcite surface is approximately 0.5 nm thick. The GEM has previously been applied to simulate uptake of elements and/or their isotopes in a number of experimental studies (*e.g.*, Mavromatis et al., 2013; 2015b; Noireaux et al., 2015; Gabitov et al., 2008; 2012; Tang et al., 2008a; 200b; 2012). Alternatively, DePaolo (2011) developed the surface reaction kinetic model (SRKM) using the principle of transition state theory (TST) to simulate elemental and isotopic fractionation during calcite growth. This model has been further extended recently (Nielsen et al., 2012, 2013; Watkins et al., 2013), and suggests a continuous change of the fractionation factor during mineral growth. This is not consistent with the mono-directional Rayleigh model used herein to estimate the fractionation factor during mineral growth, though it is worth noting that Druhan et al. (2013) suggested that a coupled ion-by-ion and reactive transport model is a better approach to a Rayleigh model in the studied groundwater system. Note also here that to date the SRKM model has been only applied to the formation of calcite in natural systems or in laboratory studies. The application of the SRKM model to elements that their masses is not limited only to two isotopomers as in the case of Ca (see Druhan et al., 2013) requires extension with respect to the system of equations that has to be solved.

In addition to growth kinetics, there are other parameters that have been shown to control isotopic fractionation during mineral growth. These include ionic strength and temperature (Watson, 1996; 2004; Dietzel et al., 2004; Tang et al., 2012), crystal structure (Mavromatis et al., 2012b, Gussone et al., 2003), as well as aqueous complexation (AlKhatib and Eisenhauer, 2016; 2017a; 2017b, Schott et al., 2016; Fujii et al., 2013; 2014; Mavromatis et al., 2017a; 2017b). Aqueous complexation effects together with the dehydration of aqueous

371 Me^{2+} ions have been shown to control fractionation between Mg-bearing carbonates and
372 reactive fluids (Schott et al., 2016). In fact, dehydration of aqueous Mg^{2+} has been suggested
373 to control both rate of crystal growth (Saldi et al., 2009; Gautier et al., 2014; 2016) and Mg
374 isotope fractionation for a variety of Mg-carbonate minerals (Pearce et al., 2012; Mavromatis
375 et al., 2013; 2017a, b; Immenhauser et al., 2010). In the case of aqueous Sr, however,
376 dehydration of the 9-coordinated aquo-ion, occurs rather fast (10^9 s^{-1}) compared to Mg (10^5 s^{-1}; Lincoln and Merbach, 1995), thus dehydration may not be of great significance for isotope
378 fractionation between aqueous Sr and strontianite. Thus the observed Sr isotope fractionation
379 during strontianite precipitation can be attributed to growth kinetics in our experiments.
380
381 4.2 Sr isotope fractionation during chemical equilibrium
382 The pH increase induced by the change from pure to atmospheric CO_2 bubbling
383 promoted rapid precipitation of strontianite, the rate of which was effectively dependent on
384 the rate of CO_2 degassing. As such, the decrease in aqueous Sr concentration closely tracked
385 the temporal evolution of pH, and near steady conditions with respect to both aqueous Sr
386 concentration and pH occurred simultaneously after ~12500 minutes as soon as chemical
387 equilibrium was achieved (Fig. 3). Yet, the $\delta^{88/86}Sr_{fluid}$ during phase II continued to evolve
388 well past the achievement of chemical equilibrium (Fig. 4). This suggests the continuous
389 exchange of Sr between strontianite and the reactive fluid at chemical equilibrium that is
390 marked by a preferential release of light ^{86}Sr from the solid to the fluid phase. The continued
391 evolution of the isotopic composition of the fluid after the attainment of chemical equilibrium
392 has previously been observed for stable Ba isotopes in the witherite-fluid system (see
393 Mavromatis et al., 2016b) and stable Mg isotopes in the magnesite-fluid system (Pearce et al.
394 2012). These observations are consistent with the concept of dynamic thermodynamic
395 chemical equilibrium. Under equilibrium conditions in a mineral-fluid system, both forward-
396 (i.e., precipitation) and back- (i.e., mineral dissolution) reactions occur, but at equal rates.

Thus the net reaction rate is zero, which results in no measurable change in elemental fluid composition. The concept of thermodynamic chemical equilibrium has been widely used to describe fluid-mineral reactions under the formulation of the transition state theory (Lasaga, 1981; Aagaard and Helgeson, 1982; Oelkers, 2001; Schott et al., 2009). In accordance with the witherite-fluid and the magnesite-fluid systems, the obtained results presented herein suggest that isotopic fractionation, in this case for Sr, is induced during mineral precipitation when the aqueous Sr is transferred to the precipitating strontianite. This results in the rapid enrichment of the fluid in ^{88}Sr observed between ~12000 and 13800 min (Fig. 4) due to the preferential uptake of ^{86}Sr into the precipitating strontianite. Near and at chemical equilibrium the rate of precipitation approaches or becomes equal to that of dissolution, which provokes the enrichment of the fluid with the lighter ^{86}Sr due to re-equilibration. At the end of the experimental run, the $\delta^{88/86}Sr_{fluid}$ does not approach that of phase I (i.e. 0.194 ‰) but is somewhat heavier, averaging at 0.400 ‰ (n=4) between 20100 and 25860 min of elapsed time (Fig. 4).

After the chemical equilibrium achieved in phase II, the $\delta^{88/86}Sr_{fluid}$ values exhibit an exponential decline that can be expressed using a relaxation curve. Similar relaxation curves have been used previously in order to estimate fluid composition changes that have been induced by jumps in experimental conditions, such as temperature-jumps (Prabhananda et al., 1987; Castaing et al., 1991), pressure-jumps (Dangles et al., 1994), and pH-jumps (Pines and Huppert, 1983; Benezeth et al., 2008). More recently we used a similar approach to explain the temporal evolution of Ba isotopes after witherite precipitation (see Mavromatis et al., 2016b). Similar to this latter study, the temporal evolution of $\delta^{88/86}Sr_{fluid}$ during phase II of the experimental run can be written as:

$$\delta^{88/86}Sr_{fluid} = y_o + Ae^{-x/\tau} \quad (5)$$

where y_o and A are constants and equal to 0.339 (±0.064) and 2.368 (±2.051) respectively, x is the reaction time (in minutes) from the onset of the experimental run and τ denotes the

relaxation time. For the experimental data shown here, τ takes the value 6233 (±3017). Note here that the use of Eq. 5 provides the means to quantify the observed isotope trend during phase II, it cannot however provide insights to the individual reaction mechanisms controlling isotope exchange. On the other hand, relaxation curves have been earlier used to define the order of reaction.

At the end of phase II, mass balance calculations suggest that the mass of strontianite remaining in the reactor was ~4.9 g, with a final measured specific area of 1.1 m^2/g, similar to that of the seed material. Considering that there are 4 atoms of Sr in each unit cell of this mineral phase, the amount of Sr in the outer surface of the strontianite present in the reactor at the end of the experiment is equal to ~0.08 mmol. Note here that for this calculation a cubic unit cell was assumed with volume equal to that of the strontianite unit cell (i.e. 259 $Å^3$) and an edge dimension of ~6.4 Å. This cubic unit cell has been used in all the calculations presented below.

The observed deviation from the Rayleigh curve at high $F_{Sr\text{-}precipitated}$, illustrated in Fig. 5, suggests a continuous exchange of Sr between the ^{86}Sr enriched strontianite and the ^{88}Sr enriched fluid. The amount of Sr released from strontianite to the fluid in order to produce its observed reduction in $\delta^{88/86}Sr_{fluid}$ can be estimated by mass balance calculations. At the chemical equilibrium that describes the strontianite-fluid system during phase II, the mass balance can be written as:

$$\delta^{88/86}Sr_{fluid-final} = \delta^{88/86}Sr_{fluid} \times (1 - f_{strontianite}) + \delta^{88/86}Sr_{strontianite} \times f_{strontianite} \quad (6)$$

where $\delta^{88/86}Sr_{fluid\text{-}final}$ and $\delta^{88/86}Sr_{fluid}$ are the final isotopic compositions of the fluid during phase II of the experiment (i.e., 0.40‰, n=4) and after the end of strontianite precipitation due to pH jump at t = 13,380 min (i.e., 0.62‰), respectively. The fraction of Sr in the aqueous phase that must be derived from exchange with strontianite after the end of precipitation is represented in Eq. (6) as $f_{strontianite}$. At the end of the experimental run, the analyzed strontianite solid had a $\delta^{88/86}Sr_{strontianite}$ of 0.154‰ (Table 1). From Eq. (6) it is calculated that to produce

449 the measured Sr stable isotopic composition of the fluid, ~47% of the Sr in the fluid phase at
450 the end of the experiment must have been derived from strontianite, despite a lack of
451 strontianite dissolution. During phase II chemical equilibrium, the average Sr in the fluid was
452 0.15 mmol, indicating that 0.08 mmol or 0.2% of the total mass of Sr present in strontianite
453 (i.e., 33.02 mmol) were exchanged with the fluid by the end of the experiment. The problem
454 with this calculation, however, is the assumption that the bulk isotopic composition of the
455 solid at the end of the experiment represents the isotopic composition of the freshly
456 precipitated strontianite. Bulk $\delta^{88/86}Sr_{strontianite}$ is consistent with the large amount of aqueous
457 Sr removed from the reactive fluid as $SrCO_3$ (see Fig. 5), which simply denotes that the bulk
458 composition of the solid at the end of the pH jump should be similar to that of the initial fluid.
459 On the other hand, the temporal evolution of the $\delta^{88/86}Sr_{fluid}$ during precipitation (Fig. 4)
460 suggests an isotopic zoning of the precipitated solid with a relative enrichment of ^{86}Sr in the
461 early precipitating layers and a progressive depletion towards the surface of the crystals. The
462 evolution of the $\delta^{88/86}Sr_{strontianite}$ as a function of Sr precipitated as strontianite that is illustrated
463 in Fig. 5 suggests that at the time the $\delta^{88/86}Sr_{fluid}$ takes its maximum value of 0.62 ‰, which
464 would equate to an instantaneous value of $\delta^{88/86}Sr_{strontianite,inst}$ for strontianite of 0.48‰. The
465 decline of the $\delta^{88/86}Sr_{fluid}$ far below this value during phase II suggests that the observed
466 isotopic exchange cannot be limited to a single surface layer, but is rather extended below it.
467 The isotopic gradient in the solid invoked by the Rayleigh distillation process makes the
468 estimation of the Sr_{solid} involved in the exchange not a straight forward process. As a first
469 approach we assume that at isotopic equilibrium during phase II the fractionation factor
470 between strontianite and fluid should be similar to that measured for phase I, i.e. $\Delta^{88/86}Sr_{solid-fluid}$ = -0.05‰. Thus the isotopic composition of the solid should be ~0.35‰ considering that
472 the measured $\delta^{88/86}Sr_{fluid}$ is 0.40‰ (Fig. 4), and assuming that this latter value represents
473 isotopic equilibrium. As calculated from the evolution of the $\delta^{88/86}Sr_{strontianite,inst}$ value (Fig. 5),
474 the amount of Sr precipitated as strontianite is 0.55 mmol. This number is ~8 times larger than

all Sr present in the external strontianite surfaces in the reactor which is calculated to be ~0.08 mmol, based on a cubic unit cell as described previously. In other words, this simplified calculation suggests that 7-8 unit cells (or ~4 nm) below the freshly precipitated strontianite surface must participate in isotopic exchange to produce the observed evolution of fluid chemistry. Note here however that this calculation assumes that all the surface sites are active, thus corresponds to the maximum moles of Sr that actually exchange with the fluid phase. As mentioned previously, these calculations include some analytical uncertainties, mainly due to the isotopic zoning in the freshly precipitated strontianite, but they nevertheless confirm that isotope exchange associated with sorption/desorption processes on the outer surface layer alone cannot explain the observed temporal evolution of the reactive fluid during phase II. Rather, it is suggested that a significant proportion (0.2 %) of the solid mass is participating in the observed isotopic exchange that takes place in phase II of the experiment.

The participation of such a large mass of the strontianite crystal suggests a mechanism of exchange with the crystal interior, rather than just the surface. The implication is that Sr is transported within the freshly precipitated crystal, either as an aqueous species within the pore space of the crystal or in the solid state, or that the outer 4 nm of the sample is dissolved and re-precipitated in place (e.g., Putnis and Mezger, 2004; Putnis, 2015). Solid-state diffusion of cations (Cd^{2+}, Ca^{2+}) has been documented to occur in calcite at 25°C at a rate on the order of nanometers in weeks (Stipp et al., 1992; Lahav and Bolt, 1964). Lahav and Bolt (1964) estimate a diffusion coefficient of 8×10^{-24} m^2/s of Ca^{2+} in calcite at 25°C. If the same diffusion coefficient is assumed for Sr^{2+} transport in strontianite and we apply the simplified diffusion equation of Stipp et al. (1992; Equation 7), which neglects particle shape, a diffusion distance of 2 nm within 8520 min is calculated (*i.e.*, the time span over which $\delta^{88/86}Sr$ is observed to stabilize during phase II) as:

$$t = {d^2}/{D} \quad (7)$$

500 where t is time, d is distance, and D is the diffusion coefficient. On the other hand, if the
501 diffusion coefficient determined by Cherniak (1997) for Sr^{2+} in calcite between 440 and
502 800°C is extrapolated to 25°C using the activation energy (1.57×10^{-36} m^2/s), a diffusion
503 distance of only 9×10^{-7} nm is calculated. The disagreement with the Cherniak (1997)
504 diffusion coefficient may be due to error in extrapolation from high to low temperature (*e.g.*,
505 Gorski and Fantle, 2017). Although it is unknown whether Sr^{2+} in strontianite exhibits a
506 similar rate of diffusion as Ca^{2+} in calcite, the better agreement between the diffusion distance
507 calculated with the Lahav and Bolt (1964) diffusion coefficient and our experimentally
508 calculated 4 nm thickness of isotopic alteration is permissive of a solid-state diffusion process
509 as an explanation for the observed isotopic exchange. It should be noted that the Lahav and
510 Bolt (1964) diffusion coefficient was determined in heterogeneous aqueous-solid systems at
511 low temperature, suggesting it may combine aqueous and solid-state diffusion or
512 dissolution/re-precipitation, compared to the Cherniak (1997) diffusion coefficient, which was
513 measured under anhydrous conditions. As such, the Lahav and Bolt (1964) diffusion
514 coefficient may better represent the conditions of our experiments.
515 With diffusion occurring at this relatively fast rate, it would nevertheless take ~3960
516 years to entirely re-equilibrate the strontianite crystals (*i.e.*, for the diffusion front to reach the
517 center of a 2 μm crystal). For a different element it has earlier been suggested that the
518 diffusion of carbon in calcite at temperatures between 250-550°C exhibits a depth-
519 dependence, with a higher diffusion coefficient in the outer-most layers due to a higher
520 density of dislocation pipes and defects (Anderson, 1969). In the case of the experiments
521 conducted in this study, mass balance calculations suggest that about 600 unit cells (or 14 %
522 of the Sr initially dissolved from the seed) re-precipitated on the surface of the crystals during
523 the pH-jump. Diffusion in these outer-most layers therefore may not reflect rates of diffusion
524 in the bulk crystal. The relatively rapid exchange observed in the upper 4 nm of the
525 strontianite crystals could be followed by a slower re-equilibration of the bulk of the crystal,

526 therefore longer timescales than calculated might be required to reset the isotopic composition
527 of the bulk crystal. Longer-term experiments are required to assess the diffusion coefficient
528 and how it may change over time. Interestingly, a relatively slow rate of diffusion of Sr within
529 the bulk crystal structure implies that the isotopic composition of the fluid will be dictated
530 largely by the isotopic composition of the surface layers of the solid, which may lead to an
531 apparent disequilibrium between the bulk solid composition and the fluid, as postulated by
532 Druhan et al (2015). Given the available data, however, it is not possible to clearly distinguish
533 the individual mechanisms of isotopic exchange, as aqueous diffusion and dissolution/re-
534 precipitation cannot be excluded.
535
536 4.3 Implications for Sr isotope signatures of natural carbonate minerals
537
538 The obtained results suggest that in the strontianite-fluid system, isotopic exchange
539 between solid and aqueous fluid proceeds at chemical equilibrium. Similar behavior has been
540 previously observed for Ba isotopes in the witherite-fluid system by Mavromatis et al.
541 (2016b) and for Mg isotopes in the magnesite-fluid system at 150 and 200^{o}C (Pearce et al.,
542 2012). Details on the mechanisms related to the observed isotopic exchange cannot be
543 extracted mainly because the above calculations are essentially based on isotopic composition
544 of the reactive fluid. It can however be inferred that the temporal evolution of the $\delta^{88/86}Sr_{fluid}$ is
545 not a result of solely a surface process such as adsorption/desorption phenomena that have
546 been earlier observed in some metal oxides and hydroxides (e.g. Barling and Anbar, 2004;
547 Wasylenki et al., 2015). Note here that the $\delta^{88/86}Sr_{fluid}$ achieves a value of 0.4‰ at the end of
548 phase II and does not evolve to lower values, although the bulk solid isotopic composition is
549 ~0.15‰, suggesting that a highly porous structure in the freshly precipitated solid cannot
550 explain the isotopic shift of the $\delta^{88/86}Sr_{fluid}$ value. Similar to the witherite-fluid system
551 (Mavromatis et al., 2016b), the results of this study are likely explained by ion mobility below

552 the crystal surface, as has been measured by Stipp and co-workers for a number of anions and
553 cations (Cd^{2+},Zn^{2+}, Na^{+}, K^{+} and Cl^{-}) near the calcite surface (Stipp et al., 1992; 1996; 1998).
554 In these studies, ion exchange was assumed to extend up to 10 atomic layers below the crystal
555 surface, which is in accordance with the ~7-8 unit cells that we estimated in this study for
556 strontianite. However, the mechanism by which the ions are transported remains unclear.
557 Isotopic re-equilibration is well known to occur at high temperatures. It has been
558 documented experimentally for Mg isotopes in magnesite (Pearce et al., 2012), and in
559 biogenic Mg-calcite (Riechelmann et al., 2016). At low temperature, isotopic exchange has
560 been observed in highly reactive hydrous Mg-carbonate minerals (Mavromatis et al., 2012a;
561 2015a; Shirokova et al. 2013), hydrous Mg-sulphates (Li et al., 2012), calcite (Avrahamov et
562 al., 2013; Mozeto et al., 1984), and redox active Fe-bearing minerals such as goethite, and
563 (Handler et al., 2009). The most important outcome of the present study, however, is the
564 observed continued exchange of Sr that alters the isotopic composition of the strontianite over
565 time. This has also been observed for witherite, and has major implications for the
566 interpretation of growth conditions of carbonates in natural archives, and the use of these
567 archives as paleoproxies. Considering that natural carbonate archives tend to stay in contact
568 with a fluid that differs in composition from the growth fluid from which they precipitated
569 their isotopic signals may be significantly reset over time. This general behavior is of great
570 interest for all carbonates phases, in particular for calcite and aragonite that are the most
571 abundant carbonate minerals, biogenic or abiogenic, in Earth's surface environments.
572 Accordingly, Fantle and DePaolo (2007) studied Ca isotopes in calcite recovered from an
573 IODP core, where Ca isotope re-equilibration between solid and fluid was postulated. Further
574 experimental work is necessitated in order to unravel the mechanisms and the extent of Me^{2+}
575 isotopic re-equilibration in carbonate minerals at temperatures encountered near the Earth's
576 surface for both constituting elements and traces/impurities. The potential secondary resetting
577 of Sr isotope signals in the Sr-endmember carbonate mineral, strontianite, hints on limitations

for the straightforward use of stable Sr isotopes in carbonate minerals as environmental or forensic proxies. On the other hand, the improved understanding of such a highly dynamic Sr isotope exchange behavior between solid and fluid at chemical equilibrium conditions may open up new proxy approaches for estimating time-resolved re-setting periods and/or explanations for zoning structures of carbonate minerals.

5. Conclusions

In this study we examined the behavior of stable Sr isotopes during the interaction of strontianite with an aqueous phase. The obtained results suggest that under isotopic equilibrium conditions the Sr isotope fractionation between strontianite and aqueous fluid is rather small but measurable and close to -0.05 ‰. This finding is in agreement with the relatively smaller Sr-O bond length in the aqueous Sr ion compared to that in strontianite. In contrast, during strontianite precipitation a preferential uptake of the ^{86}Sr isotopomer in the solid phase is observed, which is kinetically driven and is in overall agreement with the behaviour of alkali earth metals during their incorporation in carbonate minerals.

The obtained results further suggest that at chemical equilibrium conditions, a continuous exchange of Sr isotopes between solid and fluid takes place and affects at least 7-8 unit cells below the mineral surface. This observation is consistent with that observed previously for Ba isotopes in the witherite-fluid system and Mg isotopes in the magnesite-fluid system, with isotopic exchange extending up to ~10 unit cells below the crystal surface. If such a process takes place in natural aqueous settings, it likely has major implications for the secondary change of isotopic signatures of natural carbonate minerals, in particular considering that the time scales for a solid-fluid contact are significantly larger compared to the present experimental approach.

Acknowledgments

We acknowledge the assistance of Ana Kolevica for chemical preparation of the samples and their measurements at the GEOMAR mass-spectrometer facilities in Kiel, Germany and of Alain Castillo (GET, France) for his support with BET measurements. We are thankful to Bettina Purgstaller and Andre Baldermann for their support with SEM and chemical analyses. For their illuminating comments during the preparation of this manuscript we wish to thank our colleagues Florian Konrad and Cyrill Grengg. This work benefited from the constructive comments of Christopher R. Pearce and two anonymous reviewers. This study was financially supported by DFG Forschungsgruppe 1644, CHARON (IM44/10-1) and NAWI Graz.

References

Aagaard, P., Helgeson, H.C., 1982. Thermodynamic And Kinetic Constraints On Reaction-Rates Among Minerals And Aqueous-Solutions .1. Theoretical Considerations. Am. J. Sci. 282, 237-285.

Avrahamov N., Sivan O., Yechieli Y. and Lazar B., 2013. Carbon isotope exchange during calcite interaction with brine: Implications for ^{14}C dating of hypersaline groundwater. Radiocarbon 55, 81–101.

AlKhatib, M., Eisenhauer, A., 2017a. Calcium and strontium isotope fractionation during precipitation from aqueous solutions as a function of temperature and reaction rate; II. Aragonite. Geochim. Cosmochim. Acta 209, 320-342.

AlKhatib, M., Eisenhauer, A., 2017b. Calcium and strontium isotope fractionation in aqueous solutions as a function of temperature and reaction rate; I. Calcite. Geochim. Cosmochim. Acta 209, 296-319.

Anderson, T.F., 1969. Self-diffusion of carbon and oxygen in calcite by isotope exchange with carbon dioxide. J. Geophys. Res. 74, 3918-3932.

629 Barling, J., Anbar, A.D., 2004. Molybdenum isotope fractionation during adsorption by
630 manganese oxides. Earth Planet. Sci. Lett. 217, 315-329.
631 Beinlich, A., Mavromatis, V., Austrheim, H., Oelkers, E.H., 2014. Inter-mineral Mg isotope
632 fractionation during hydrothermal ultramafic rock alteration – Implications for the
633 global Mg-cycle. Earth Planet. Sci. Lett. 392, 166-176.
634 Benezeth, P., Palmer, D.A., Wesolowski, D.J., 2008. Dissolution/precipitation kinetics of
635 boehmite and gibbsite: Application of a pH-relaxation technique to study near-
636 equilibrium rates. Geochim. Cosmochim. Acta 72, 2429-2453.
637 Böhm, F., Eisenhauer, A., Tang, J., Dietzel, M., Krabbenhoeft, A., Kisakürek, B., Horn, C.,
638 2012. Strontium isotope fractionation of planktic foraminifera and inorganic calcite.
639 Geochim. Cosmochim. Acta 93, 300-314.
640 Böttcher, M.E., Geprags, P., Neubert, N., von Allmen, K., Pretet, C., Samankassou, E.,
641 Nagler, T.F., 2012. Barium isotope fractionation during experimental formation of the
642 double carbonate $BaMn(CO_3)_2$ at ambient temperature. Isot. Environ. Health Stud. 48,
643 457-463.
644 Brunauer, S., Emmett, P.H., Teller, E., 1938. Adsorption of Gasses in Multimolecular layers.
645 Journal of American Chemical Society 60, 309-319.
646 Busenberg, E., Plummer, L.N., Parker, V.B., 1984. The solubility of strontianite ($SrCO_3$) in
647 CO_2-H_2O solutions between 2 and 91 ^oC, the association constants of $SrHCO_3^+$ (aq) and
648 $SrCO_3^o$ (aq) between 5 and 80 ^oC, and an evaluation of the thermodynamic properties of
649 Sr^{2+} (aq) and $SrCO_3$(cr) at 25 ^oC and 1 atm total pressure. Geochim. Cosmochim. Acta
650 48, 2021-2035.
651 Castaing, M., Kraus, J.L., Beaufils, P., Ricard, J., 1991. Temperature-jump method for
652 studying the fast transport of Na^+ by (221)c10-cryptand across lipid-membranes.
653 Biophys. Chem. 41, 203-215.

654 Cherniak D.J. 1997. An experimental study of strontium and lead diffusion in calcite, and
655 implications for carbonate diagenesis and metamorphism. Geochim. Cosmochim. Acta
656 61, 4173-4179.
657 Criss R. E. 1999. Principles of Stable Isotope Distribution. Oxford University Press, Oxford.
658 D'Angelo, P., Migliorati, V., Sessa, F., Mancini, G., Persson, I., 2016. XANES Reveals the
659 Flexible Nature of Hydrated Strontium in Aqueous Solution. J. Phys. Chem. B 120,
660 4114-4124.
661 Dangles, O., Elhabiri, M., Brouillard, R., 1994. Kinetic and thermodynamic investigation of
662 the aluminum anthocyanin complexation in aqueous-solution. J. Chem. Soc.-Perkin
663 Trans. 2, 2587-2596.
664 DePaolo, D.J., 2011. Surface kinetic model for isotopic and trace element fractionation during
665 precipitation of calcite from aqueous solutions. Geochim. Cosmochim. Acta 75, 1039-
666 1056.
667 Dietzel, M., Gussone, N., Eisenhauer, A., 2004. Co-precipitation of Sr^{2+} and Ba^{2+} with
668 aragonite by membrane diffusion of CO_2 between 10 and 50 ^{o}C. Chem. Geol. 203, 139-
669 151.
670 Dietzel, M., Schön, F., Heinrichs, J., Deditius, A.P., Leis, A. (2016) Tracing formation and
671 durability of calcite in a Punic-Roman cistern mortar (Pantelleria Island, Italy). Isotopes
672 in Health Study 52, 112-127.
673 Druhan, J.L., Steefel, C.I., Williams, K.H., DePaolo, D.J., 2013. Calcium isotope
674 fractionation in groundwater: Molecular scale processes influencing field scale
675 behavior. Geochim. Cosmochim. Acta 119, 93-116.
676 Eisenhauer, A., Kisakurek, B., Bohm, F., 2009. Marine Calcification: An Alkaline Earth
677 Metal Isotope Perspective. Elements 5, 365-368.
678 Fantle, M.S., DePaolo, D.J., 2007. Ca isotopes in carbonate sediment and pore fluid from
679 ODP Site 807A: The Ca^{2+}(aq)-calcite equilibrium fractionation factor and calcite

680 recrystallization rates in Pleistocene sediments. Geochim. Cosmochim. Acta 71, 2524-
681 2546.
682 Fruchter, N., Eisenhauer, A., Dietzel, M., Fietzke, J., Böhm, F., Montagna, P., Stein, M.,
683 Lazar, B., Rodolfo-Metalpa, R., Erez, J., 2016. $^{88}Sr/^{86}Sr$ fractionation in inorganic
684 aragonite and in corals. Geochim. Cosmochim. Acta 178, 268-280.
685 Fujii, T., Moynier, F., Abe, M., Nemoto, K., Albarede, F., 2013. Copper isotope fractionation
686 between aqueous compounds relevant to low temperature geochemistry and biology.
687 Geochim. Cosmochim. Acta 110, 29-44.
688 Fujii, T., Moynier, F., Blichert-Toft, J., Albarede, F., 2014. Density functional theory
689 estimation of isotope fractionation of Fe, Ni, Cu, and Zn among species relevant to
690 geochemical and biological environments. Geochim. Cosmochim. Acta 140, 553-576.
691 Gabitov, R.I., Gaetani, G.A., Watson, E.B., Cohen, A.L., Ehrlich, H.L., 2008. Experimental
692 determination of growth rate effect on U^{6+} and Mg^{2+} partitioning between aragonite and
693 fluid at elevated U^{6+} concentration. Geochim. Cosmochim. Acta 72, 4058-4068.
694 Gabitov, R.I., Watson, E.B., Sadekov, A., 2012. Oxygen isotope fractionation between calcite
695 and fluid as a function of growth rate and temperature: An in situ study. Chem. Geol.
696 306, 92-102.
697 Gautier, Q., Bénézeth, P., Mavromatis, V., Schott, J., 2014. Hydromagnesite solubility
698 product and growth kinetics in aqueous solution from 25 to 75°C. Geochim.
699 Cosmochim. Acta 138, 1-20.
700 Gautier, Q., Bénézeth, P., Schott, J., 2016. Magnesite growth inhibition by organic ligands:
701 An experimental study at 100, 120 and 146 °C. Geochim. Cosmochim. Acta 181, 101-
702 125.
703 Geske, A., Goldstein, R.H., Mavromatis, V., Richter, D.K., Buhl, D., Kluge, T., John, C.M.,
704 Immenhauser, A., 2015. The magnesium isotope ($\delta^{26}Mg$) signature of dolomites.
705 Geochim. Cosmochim. Acta 149, 131-151.

706 Gorski, C.A., Fantle, M.S., 2017. Stable mineral recrystallization in low temperature aqueous
707 systems: A critical review. Geochim. Cosmochim. Acta 198, 439-465.
708 Gussone, N., Eisenhauer, A., Heuser, A., Dietzel, M., Bock, B., Boehm, F., Spero, H.J., Lea,
709 D.W., Bijma, J., Naegler, T.F., 2003. Model for kinetic effects on calcium isotope
710 fractionation $\delta^{44}Ca$ in inorganic aragonite and cultured planktonic Foraminifera.
711 Geochim. Cosmochim. Acta 67, 1375-1382.
712 Handler R. M., Beard B. L., Johnson C. M. and Scherer M. M., 2009. Atom exchange
713 between aqueous Fe(II) and goethite: an Fe isotope tracer study. Environ. Sci. Technol.
714 43, 1102–1107.
715 Heuser, A., Eisenhauer, A., 2010. A pilot study on the use of natural calcium isotope
716 ($^{44}Ca/^{40}Ca$) fractionation in urine as a proxy for the human body calcium balance. Bone
717 46, 889-896.
718 Holl, C.M., Smyth, J.R., Laustsen, H.M.S., Jacobsen, S.D., Downs, R.T., 2000. Compression
719 of witherite to 8 Gpa and the crystal structure of $BaCO_3$ II. Phys. Chem. Miner. 27, 467-
720 473.
721 Immenhauser, A., Buhl, D., Richter, D., Niedermayr, A., Riechelmann, D., Dietzel, M.,
722 Schulte, U., 2010. Magnesium-isotope fractionation during low-Mg calcite precipitation
723 in a limestone cave - Field study and experiments. Geochim. Cosmochim. Acta 74,
724 4346-4364.
725 Krabbenhöft, A., Fietzke, J., Eisenhauer, A., Liebetrau, V., Böhm, F., Vollstaedt, H., 2009.
726 Determination of radiogenic and stable strontium isotope ratios ($^{87}Sr/^{86}Sr$; $\delta^{88/86}Sr$) by
727 thermal ionization mass spectrometry applying an $^{87}Sr/^{84}Sr$ double spike. J. Anal. At.
728 Spectrom. 24, 1267-1271.
729 Lahav, N., Bolt, G.H., 1964. Self-diffusion of ca45 into certain carbonates. Soil Sci. 97, 293-
730 299.
731 Lasaga A. C. (1981) Transition state theory. Rev. Mineral. 8, 135– 169.

732 Li, W., Beard, B.L., Li, C., Johnson, C.M., 2014. Magnesium isotope fractionation between
733 brucite $Mg(OH)_2$ and Mg aqueous species: Implications for silicate weathering and
734 biogeochemical processes. Earth Planet. Sci. Lett. 394, 82-93.
735 Li, W., Beard, B.L., Li, C., Xu, H., Johnson, C.M., 2015. Experimental calibration of Mg
736 isotope fractionation between dolomite and aqueous solution and its geological
737 implications. Geochim. Cosmochim. Acta 157, 164-181.
738 Li, W., Chakraborty, S., Beard, B.L., Romanek, C.S., Johnson, C.M., 2012. Magnesium
739 isotope fractionation during precipitation of inorganic calcite under laboratory
740 conditions. Earth Planet. Sci. Lett. 333-334, 304-316.
741 Li, W.Q., Beard, B.L., Johnson, C.M., 2011. Exchange and fractionation of Mg isotopes
742 between epsomite and saturated $MgSO_4$ solution. Geochim. Cosmochim. Acta 75,
743 1814-1828.
744 Lincoln, S.F., Merbach, A.E., 1995. Substitution Reactions of Solvated Metal Ions, in: Sykes,
745 A.G. (Ed.), Advances in Inorganic Chemistry. Academic Press, pp. 1-88.
746 Mavromatis, V., Bundeleva, I.A., Shirokova, L.S., Millo, C., Pokrovsky, O.S., Bénézeth, P.,
747 Ader, M., Oelkers, E.H., 2015a. The continuous re-equilibration of carbon isotope
748 compositions of hydrous Mg carbonates in the presence of cyanobacteria. Chem. Geol.
749 404, 41-51.
750 Mavromatis, V., Gautier, Q., Bosc, O., Schott, J., 2013. Kinetics of Mg partition and Mg
751 stable isotope fractionation during its incorporation in calcite. Geochim. Cosmochim.
752 Acta 114, 188-203.
753 Mavromatis, V., Montouillout, V., Noireaux, J., Gaillardet, J., Schott, J., 2015b.
754 Characterization of boron incorporation and speciation in calcite and aragonite from co-
755 precipitation experiments under controlled pH, temperature and precipitation rate.
756 Geochim. Cosmochim. Acta 150, 299-313.

Mavromatis, V., Pearce, C.R., Shirokova, L.S., Bundeleva, I.A., Pokrovsky, O.S., Benezeth, P., Oelkers, E.H., 2012a. Magnesium isotope fractionation during hydrous magnesium carbonate precipitation with and without cyanobacteria. Geochim. Cosmochim. Acta 76, 161-174.

Mavromatis, V., Rinder, T., Prokushkin, A.S., Pokrovsky, O.S., Korets, M.A., Chmeleff, J., Oelkers, E.H., 2016a. The effect of permafrost, vegetation, and lithology on Mg and Si isotope composition of the Yenisey River and its tributaries at the end of the spring flood. Geochim. Cosmochim. Acta 191, 32-46.

Mavromatis, V., Schmidt, M., Botz, R., Comas-Bru, L., Oelkers, E.H., 2012b. Experimental quantification of the effect of Mg on calcite-aqueous fluid oxygen isotope fractionation. Chem. Geol. 310-311, 97-105.

Mavromatis, V., van Zuilen, K., Purgstaller, B., Baldermann, A., Nägler, T.F., Dietzel, M., 2016b. Barium isotope fractionation during witherite ($BaCO_3$) dissolution, precipitation and at equilibrium. Geochim. Cosmochim. Acta 190, 72-84.

Mavromatis, V., Immenhauser, A., Buhl, D., Purgstaller, B., Baldermann, A., Dietzel, M., 2017b. Effect of organic ligands on Mg partitioning and Mg isotope fractionation during low-temperature precipitation of calcite in the absence of growth rate effects. Geochim. Cosmochim. Acta 207, 139-153.

Mavromatis, V., Prokushkin, A.S., Pokrovsky, O.S., Viers, J., Korets, M.A., 2014. Magnesium isotopes in permafrost-dominated Central Siberian larch forest watersheds. Geochim. Cosmochim. Acta 147, 76-89.

Mavromatis, V., Purgstaller, B., Dietzel, M., Buhl, D., Immenhauser, A., Schott, J., 2017a. Impact of amorphous precursor phases on magnesium isotope signatures of Mg-calcite. Earth Planet. Sci. Lett. 464, 227-236.

781 Meheut, M., Lazzeri, M., Balan, E., Mauri, F., 2007. Equilibrium isotopic fractionation in the
782 kaolinite, quartz, water system: Prediction from first-principles density-functional
783 theory. Geochim. Cosmochim. Acta 71, 3170-3181.
784 Mozeto, A.A., Fritz, P., Reardon, E.J., 1984. Experimental-observations on carbon isotope
785 exchange in carbonate-water systems. Geochim. Cosmochim. Acta 48, 495-504.
786 Nielsen, L.C., De Yoreo, J.J., DePaolo, D.J., 2013. General model for calcite growth kinetics
787 in the presence of impurity ions. Geochim. Cosmochim. Acta 115, 100-114.
788 Nielsen, L.C., DePaolo, D.J., De Yoreo, J.J., 2012. Self-consistent ion-by-ion growth model
789 for kinetic isotopic fractionation during calcite precipitation. Geochim. Cosmochim.
790 Acta 86, 166-181.
791 Noireaux, J., Mavromatis, V., Gaillardet, J., Schott, J., Montouillout, V., Louvat, P., Rollion-
792 Bard, C., Neuville, D.R., 2015. Crystallographic control on the boron isotope paleo-pH
793 proxy. Earth Planet. Sci. Lett. 430, 398-407.
794 O'Day, P.A., Newville, M., Neuhoff, P.S., Sahai, N., Carroll, S.A., 2000. X-ray absorption
795 spectroscopy of strontium(II) coordination - I. Static and thermal disorder in crystalline,
796 hydrated, and precipitated solids and in aqueous solution. J. Colloid Interface Sci. 222,
797 184-197.
798 Oelkers, E.H., 2001. General kinetic description of multioxide silicate mineral and glass
799 dissolution. Geochim. Cosmochim. Acta 65, 3703-3719.
800 Pearce, C.R., Saldi, G.D., Schott, J., Oelkers, E.H., 2012. Isotopic fractionation during
801 congruent dissolution, precipitation and at equilibrium: Evidence from Mg isotopes.
802 Geochim. Cosmochim. Acta 92, 170-183.
803 Persson, I., Sandstrom, M., Yokoyama, H., Chaudhry, M., 1995. Structure of the solvated
804 strontium and barium ions in aqueous, dimethyl-sulfoxide and pyridine solution, and
805 crystal-structure of strontium and barium hydroxide octahydrate. Z. Naturfors. Sect. A-
806 J. Phys. Sci. 50, 21-37.

807 Pines, E., Huppert, D., 1983. pH Jump - a Relaxational Approach. J. Phys. Chem. 87, 4471-
808 4478.
809 Pinilla, C., Blanchard, M., Balan, E., Natarajan, S.K., Vuilleumier, R., Mauri, F., 2015.
810 Equilibrium magnesium isotope fractionation between aqueous Mg2+ and carbonate
811 minerals: Insights from path integral molecular dynamics. Geochim. Cosmochim. Acta
812 163, 126-139.
813 Plummer, L.N., Busenberg, E., 1987. Thermodynamics of aragonite-strontianite solid
814 solutions: Results from stoichiometric solubility at 25 and 76°C. Geochim. Cosmochim.
815 Acta 51, 1393-1411.
816 Plummer, L.N., Busenberg, E., Glynn, P.D., Blum, A.E., 1992. Dissolution of aragonite-
817 strontianite solid-solutions in nonstoichiometric $Sr(HCO_3)_2$-$Ca(HCO_3)_2$-CO_2-H_2O
818 solutions. Geochim. Cosmochim. Acta 56, 3045-3072.
819 Pokrovsky, B.G., Mavromatis, V., Pokrovsky, O.S., 2011. Co-variation of Mg and C isotopes
820 in late Precambrian carbonates of the Siberian Platform: A new tool for tracing the
821 change in weathering regime? Chem. Geol. 290, 67-74.
822 Prabhananda, B.S., Rittger, E., Grell, E., 1987. Kinetics and mechanism of anionic ligand-
823 binding to carbonic-anhydrase. Biophys. Chem. 26, 217-224.
824 Riechelmann, S., Mavromatis, V., Buhl, D., Dietzel, M., Eisenhauer, A., Immenhauser, A.,
825 2016. Impact of diagenetic alteration on brachiopod shell magnesium isotope ($\delta^{26}Mg$)
826 signatures: Experimental versus field data. Chem. Geol. 440, 191-206.
827 Rollion-Bard, C., Blamart, D., Trebosc, J., Tricot, G., Mussi, A., Cuif, J.P., 2011. Boron
828 isotopes as pH proxy: A new look at boron speciation in deep-sea corals using B-11
829 MAS NMR and EELS. Geochim. Cosmochim. Acta 75, 1003-1012.
830 Rollion-Bard, C., Saulnier, S., Vigier, N., Schumacher, A., Chaussidon, M., Lecuyer, C.,
831 2016. Variability in magnesium, carbon and oxygen isotope compositions of brachiopod
832 shells: Implications for paleoceanographic studies. Chem. Geol. 423, 49-60.

833 Rustad, J.R., Casey, W.H., Yin, Q.Z., Bylaska, E.J., Felmy, A.R., Bogatko, S.A., Jackson,
834 V.E., Dixon, D.A., 2010. Isotopic fractionation of Mg^{2+}(aq), Ca^{2+}(aq), and Fe^{2+}(aq) with
835 carbonate minerals. Geochim. Cosmochim. Acta 74, 6301-6323.
836 Saldi, G.D., Jordan, G., Schott, J., Oelkers, E.H., 2009. Magnesite growth rates as a function
837 of temperature and saturation state. Geochim. Cosmochim. Acta 73, 5646-5657.
838 Schauble, E.A., 2011. First-principles estimates of equilibrium magnesium isotope
839 fractionation in silicate, oxide, carbonate and hexaaquamagnesium(2+) crystals.
840 Geochim. Cosmochim. Acta 75, 844-869.
841 Schott, J., Mavromatis, V., Fujii, T., Pearce, C.R., Oelkers, E.H., 2016. The control of
842 carbonate mineral Mg isotope composition by aqueous speciation: Theoretical and
843 experimental modeling. Chem. Geol. 445, 120-134.
844 Schott, J., Pokrovsky, O.S., Oelkers, E.H., 2009. The Link between Mineral
845 Dissolution/Precipitation Kinetics and Solution Chemistry, in: Oelkers, E.H., Schott, J.
846 (Eds.), Thermodynamics and Kinetics of Water-Rock Interaction. Mineralogical Soc
847 Amer, pp. 207-258.
848 Shirokova, L.S., Mavromatis, V., Bundeleva, I.A., Pokrovsky, O.S., Benezeth, P., Gerard, E.,
849 Pearce, C.R., Oelkers, E.H., 2013. Using Mg Isotopes to Trace Cyanobacterially
850 Mediated Magnesium Carbonate Precipitation in Alkaline Lakes. Aquat. Geochem. 19,
851 1-24.
852 Skulan, J.L., Beard, B.L., Johnson, C.M., 2002. Kinetic and equilibrium Fe isotope
853 fractionation between aqueous Fe(III) and hematite. Geochim. Cosmochim. Acta 66,
854 2995-3015.
855 Speer (1983) Crystal chemistry and phase relations of orthorhombic carbonates. In Reviews
856 in Mineralogy: Carbonates –Mineralogy and Chemistry (ed. R. J. Reeder), pp. 145–189.
857 Stipp, S.L., Hochella, M.F., Parks, G.A., Leckie, J.O., 1992. Cd2+ uptake by calcite, solid-
858 state diffusion, and the formation of solid-solution - interface processes observed with

near-surface sensitive techniques (XPS, LEED, and AES). Geochim. Cosmochim. Acta 56, 1941-1954.

Stipp, S.L.S., Gutmannsbauer, W., Lehmann, T., 1996. The dynamic nature of calcite surfaces in air. Am. Miner. 81, 1-8.

Stipp, S.L.S., Konnerup-Madsen, J., Franzreb, K., Kulik, A., Mathieu, H.J., 1998. Spontaneous movement of ions through calcite at standard temperature and pressure. Nature 396, 356-359.

Tang, J., Dietzel, M., Böhm, F., Köhler, S.J., Eisenhauer, A., 2008a. Sr^{2+}/Ca^{2+} and $^{44}Ca/^{40}Ca$ fractionation during inorganic calcite formation: II. Ca isotopes. Geochim. Cosmochim. Acta 72, 3733-3745.

Tang, J., Köhler, S.J., Dietzel, M., 2008b. Sr^{2+}/Ca^{2+} and $^{44}Ca/^{40}Ca$ fractionation during inorganic calcite formation: I. Sr incorporation. Geochim. Cosmochim. Acta 72, 3718-3732.

Tang, J.W., Niedermayr, A., Köhler, S.J., Böhm, F., Kisakurek, B., Eisenhauer, A., Dietzel, M., 2012. Sr^{2+}/Ca^{2+} and $^{44}Ca/^{40}Ca$ fractionation during inorganic calcite formation: III. Impact of salinity/ionic strength. Geochim. Cosmochim. Acta 77, 432-443.

Vigier, N., Rollion-Bard, C., Levenson, Y., Erez, J., 2015. Lithium isotopes in foraminifera shells as a novel proxy for the ocean dissolved inorganic carbon (DIC). C. R. Geosci. 347, 43-51.

Wasylenki, L.E., Howe, H.D., Spivak-Birndorf, L.J., Bish, D.L., 2015. Ni isotope fractionation during sorption to ferrihydrite: Implications for Ni in banded iron formations. Chem. Geol. 400, 56-64.

Watkins, J.M., Nielsen, L.C., Ryerson, F.J., DePaolo, D.J., 2013. The influence of kinetics on the oxygen isotope composition of calcium carbonate. Earth Planet. Sci. Lett. 375, 349-360.

884 Watson, E.B., Liang, Y., 1995. A simple model for sector zoning in slowly grown crystals:
885 Implications for growth rate and lattice diffusion, with emphasis on accessory minerals
886 in crustal rocks. Am. Miner. 80, 1179-1187.
887 Watson, E.B., 1996. Surface enrichment and trace-element uptaking during crystal growth.
888 Geochim. Cosmochim. Acta 60, 5013-5020.
889 Watson, E.B., 2004. A conceptual model for near-surface kinetic controls on the trace-
890 element and stable isotope composition of abiogenic calcite crystals. Geochim.
891 Cosmochim. Acta 68, 1473-1488.
892

Table 1: Strontium concentration, Sr isotope composition, pH and saturation degree with respect to strontianite in fluid samples and stable Sr isotope composition of solids and reference materials analyzed in this study for experiment 1. r_p: growth rate of strontianite calculated according to equation (3). The sample $SrCl_2$ – synthesis refers to composition of the fluid used for the synthesis of strontianite.

Elapsed Time (min)	Sr (mM)	pH	$\Omega_{strontianite}$	Alkalinity (mM)	R_p (mol/m^2/s)	$\delta^{88/86}$Sr (‰)	2sd	$^{87/86}$Sr
0		6.00						
1500	5.08	5.90	1.16	7.51		0.191	0.005	0.708541
2880	5.08	5.88	1.12	7.59				
4260	4.86	5.94	1.20	7.33		0.200	0.003	0.708548
5820	4.96	5.92	1.20	7.54				
7140	4.89	5.91	1.12	7.32		0.193	0.008	0.708537
8700	4.87	5.91	1.15	7.53		0.198	0.004	0.708546
10080	4.72	5.96	1.24	7.47				
11580	4.87	5.94	1.23	7.54				
12540	4.76	5.93	1.18	7.58		0.187	0.011	0.708538
12660	4.29	6.15	1.55	6.43	1.5E-09	0.167	0.004	0.708544
12780	3.27	6.35	1.41	4.57	3.0E-09	0.202	0.005	0.708543
12840	2.27	6.81	2.07	3.17	5.5E-09	0.227	0.002	0.708540
12930	0.76	7.50	2.71	2.41	5.1E-09	0.298	0.010	0.708540
13020	0.47	7.64	2.22	2.28	9.5E-10	0.508	0.003	0.708540
13380	0.27	7.84	1.83	2.08	1.7E-10	0.590	0.004	0.708540
14340	0.21	7.96	1.59	1.71	1.8E-11	0.622	0.003	0.708547
15960	0.17	8.00	1.13	1.36	7.7E-12	0.597	0.004	0.708541
17280	0.17	8.05	1.16	1.21	7.8E-14	0.527	0.002	0.708744
18720	0.18	7.93	0.93	1.22		0.538	0.007	0.708539
20100	0.23	7.91	1.07	1.16		0.475	0.009	0.708704
21540	0.22	7.89	1.05	1.26		0.428	0.008	0.708534
24420	0.19	7.98	1.04	1.15		0.369	0.003	0.708545
25860	0.14	8.10	1.02	1.14		0.387	0.006	0.708699
Strontianite seed						0.145	0.003	0.708542
Strontianite after dissolution						0.167	0.004	0.708542
Strontianite final						0.154	0.002	0.708542
$SrCl_2$ - synthesis						0.154	0.013	0.708543

901 Figure 1

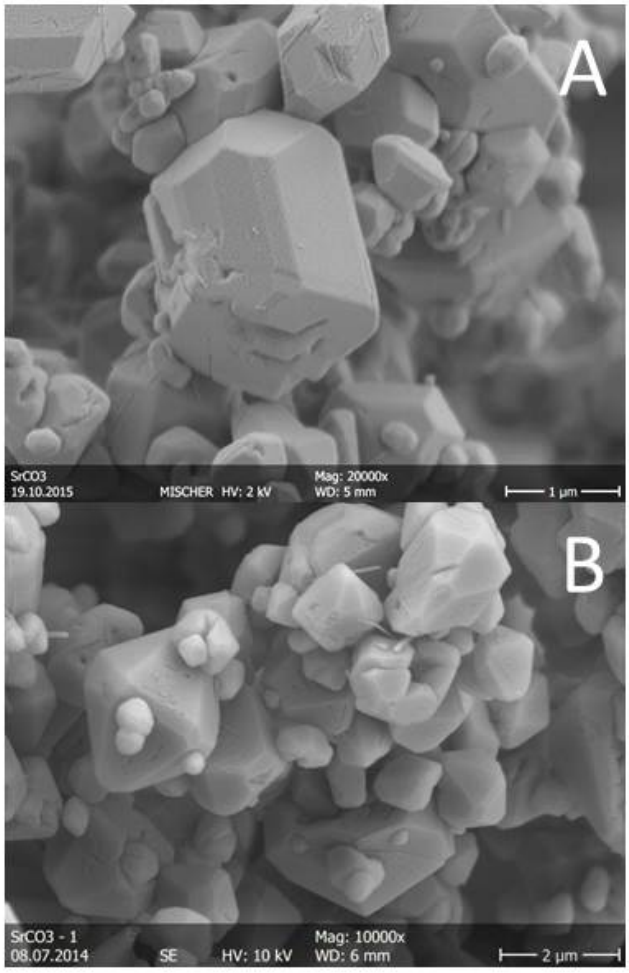

902

903 Figure 1: Scanning electron microscopy images of strontianite seeds (A) and strontianite
904 collected at the end of the experimental run (B). No significant changes in the shape and
905 surface texture of strontianite occurred during the course of the experiment.
906

907 Figure 2
908

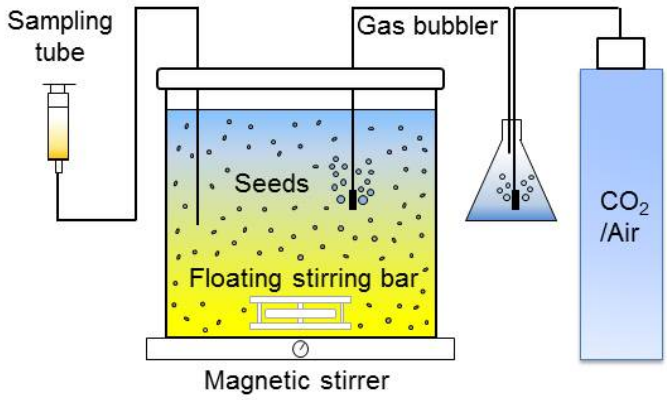

909
910
911 Figure 2: Experimental setup (modified after Mavromatis et al., 2016)
912

913 Figure 3
914

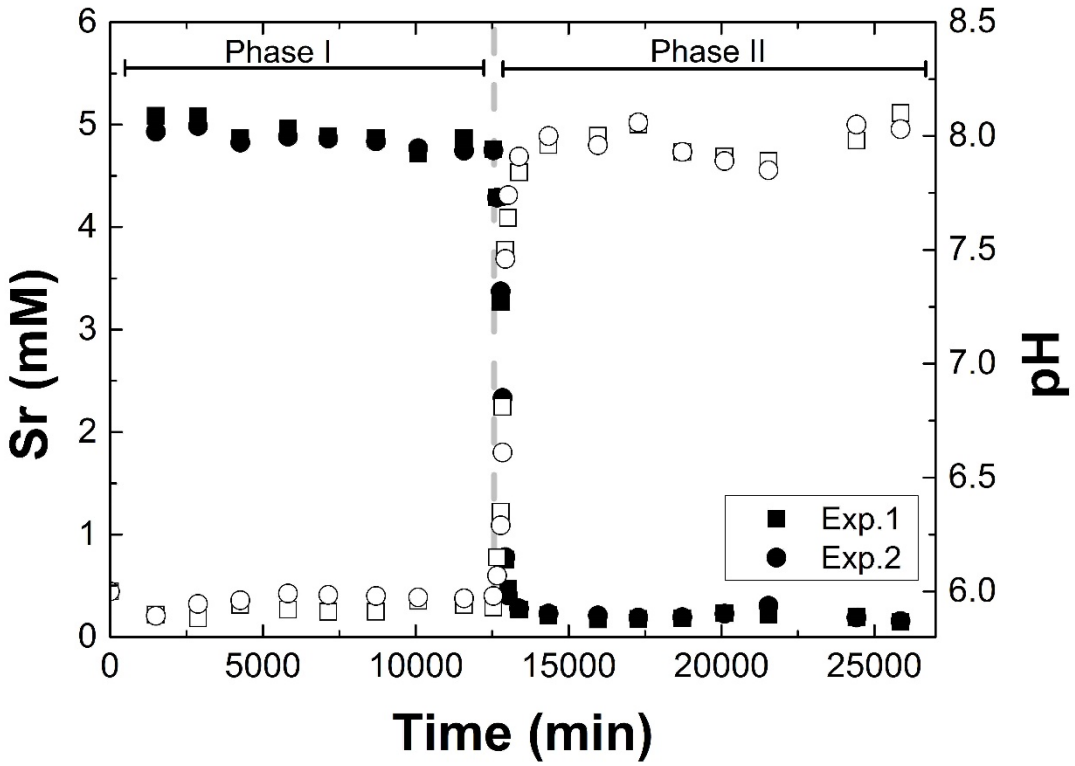

915
916 Fig. 3: Temporal evolution of Sr concentration (closed symbols) and pH (open symbols) in
917 the two replicate experimental runs. The dashed gray line indicates the transition in bubbling
918 from CO_2 to atmospheric air. Analytical uncertainty is smaller than symbol size.

919

920

921 Figure 4

922

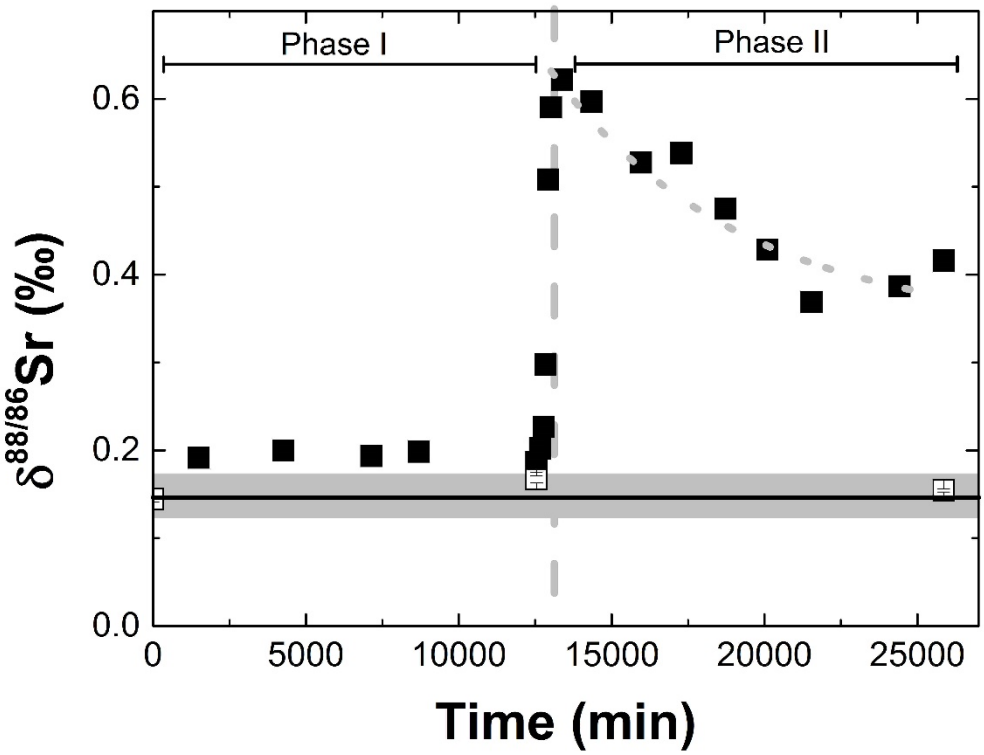

923
924
925 Figure 4: Temporal evolution of $\delta^{88/86}$Sr values of Sr ions in the reactive fluid. The white
926 points represent the $\delta^{88/86}$Sr value of the strontianite in the reactor. Analytical uncertainty is
927 included in the symbol size.
928

Figure 5

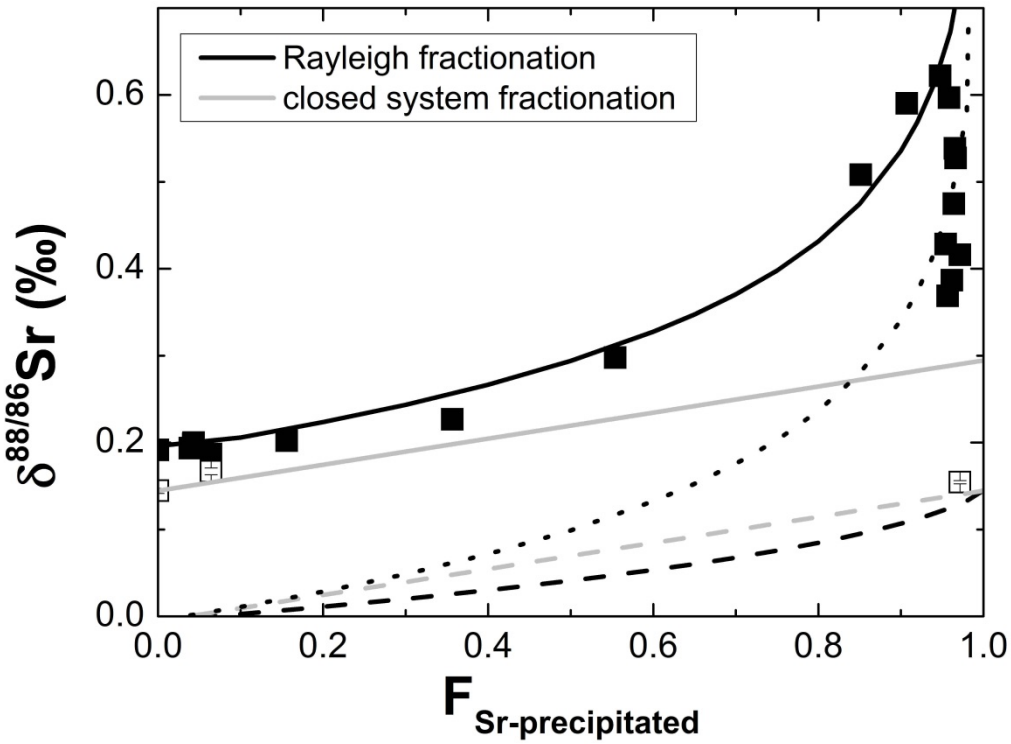

Figure 5: $\delta^{88/86}Sr_{fluid}$ values (■) plotted as a function of the molar fraction of Sr precipitated as strontianite. (□): $\delta^{88/86}Sr_{SrCO3}$ values of the solid phase. The dashed lines indicate the theoretical evolution of the isotopic composition of the cumulated solid phase, whereas the dotted line indicates the instant isotopic composition of the precipitating solid. The fractionation factor used for both models, Rayleigh and closed system, is $\alpha = 0.99985$.